Available online at www.sciencedirect.com
SCIENCE DIRECT®
Computers and electronics in agriculture
Computers and Electronics in Agriculture 41 (2003) 121–137
www.elsevier.com/locate/compag

Surface shape analysis of rough lumber for wane detection

Sang-Mook Lee [a,*], A. Lynn Abbott [a], Daniel L. Schmoldt [b]

[a] *Bradley Department of Electrical and Computer Engineering, Virginia Tech, Blacksburg, VA 24061, USA*
[b] *USDA Cooperative State Research, Education, and Extension Service (CSREES), 800 9th Street SW, Waterfront Centre, Room 3122, Washington, DC 20024, USA*

Abstract

The initial breakdown of hardwood logs into lumber produces boards with rough surfaces. These boards contain wane (missing wood that emanates from the log exterior, often containing residual bark) that is removed by edge and trim cuts prior to sale. Because hardwood lumber value is determined based on board size and quality, knowledge of wane position and defects is essential for selecting cuts that maximize profit. We have developed a system that uses structured light to obtain profile (thickness) images of unplaned boards, in addition to gray-scale images for defect detection. The focus of this paper is to describe a new approach for detecting wane boundaries through the analysis of these profile images. The problem is difficult because bark and other debris adversely affect the laser-based imaging process, and because variations in surface reflectance also cause inaccuracies in the measured thickness values. The problem is compounded by the need to perform wane detection rapidly in a manufacturing environment. The method that we have developed relies on a combination of column-wise image statistics, selective smoothing, and the analysis of surface shape. Initial wane edge estimates that are obtained using the smoothed image are then refined by analysis of the original image data. The paper provides a quantitative evaluation that indicates a dramatic improvement over traditional thresholding techniques.

Keywords: Hardwood; Wane detection; Shape estimation

* Corresponding author.
E-mail addresses: lsmook@vt.edu (S.-M. Lee), abbott@vt.edu (A.s. Abbott), dschmoldt@reeusda.gov (D. Schmoldt).

0168-1699/03/$ - see front matter
doi:10.1016/S0168-1699(03)00047-4

1. Introduction

In present-day hardwood sawmills, logs are first cut into boards that retain wane (residual bark regions) and other undesirable features of the log. Edger and trimmer operators then visually examine the surfaces of each board, and make quick judgments about the placement of cuts based on their knowledge of lumber grades and current lumber prices. Ideally, edge and trim cuts will be selected so that the sale value of each board is maximized. In practice, however, optimizing the value of each board in this manner is a complex decision that is difficult even for experienced operators. The decision is based on the position of wane and defects, as well as current market prices for wood.

Work is in progress to develop a prototype scanning system that can determine optimum edging and trimming solutions for rough (unplaned) hardwood boards (Lee et al., 1999). Except for some earlier work (Conners et al., 1989; Cho et al., 1990a,b)—which subsequently abandoned the rough lumber problem and looked instead at surfaced lumber—little has been done to address the image analysis problems associated with rough lumber. This paper particularly addresses the problem of automatically detecting wane on rough hardwood lumber. This capability, together with automatic defect detection, will form the nucleus of computer-driven edging and trimming. As described in Section 2 of this paper, the scanning system captures *profile* images (or, equivalently, *range* images) using a laser source and a video camera, so that each pixel represents a measurement of board thickness. As an example, a portion of a profile image is given in Fig. 1.

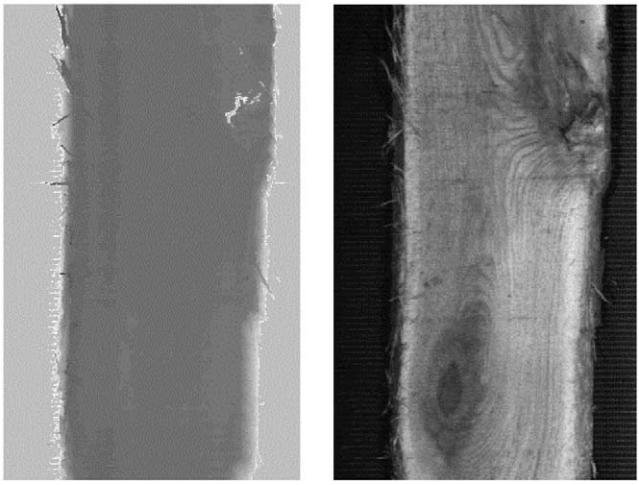

Fig. 1. Registered range and intensity images for a rough board. (a) Example range image, in which darker areas represent points on the board that are closer to the camera. (b) Corresponding intensity image, for which each pixel represents the intensity of reflected light.

At first glance, the detection of wane would appear to be a relatively simple problem involving the selection of a threshold thickness value in the profile image. Although this approach might be adequate for some applications, the problem is difficult for unplaned lumber because images are typically contaminated by several types of noise. Our approach to the detection of wane is to search for discontinuities in surface characteristics of the wood. Smoothing operations are employed to reduce the effects of noise, and features derived from surface curvature and surface-normal direction are used to localize wane boundaries.

After describing the imaging system, the paper presents additional details on the types of noise that are present. The subsequent sections describe our wane-detection method analytically, present experimental results with error analysis, and provide concluding remarks.

2. Data acquisition

In a widely used technique known as sheet-of-light profile imaging (Fig. 2), a plane of light is generated onto an uneven surface. Light that reflects from the surface appears as a 2-dimensional curve in an image, when viewed from an angle relative to the light plane. By using triangulation, it is possible to estimate thickness values over the surface of the object. Because many lumber defects (e.g. voids, wane, twist, and splits) are associated with surface irregularities, profiling is extremely useful in wood applications. In addition, it is possible to obtain intensity information simultaneously that is exactly correlated spatially with profile information.

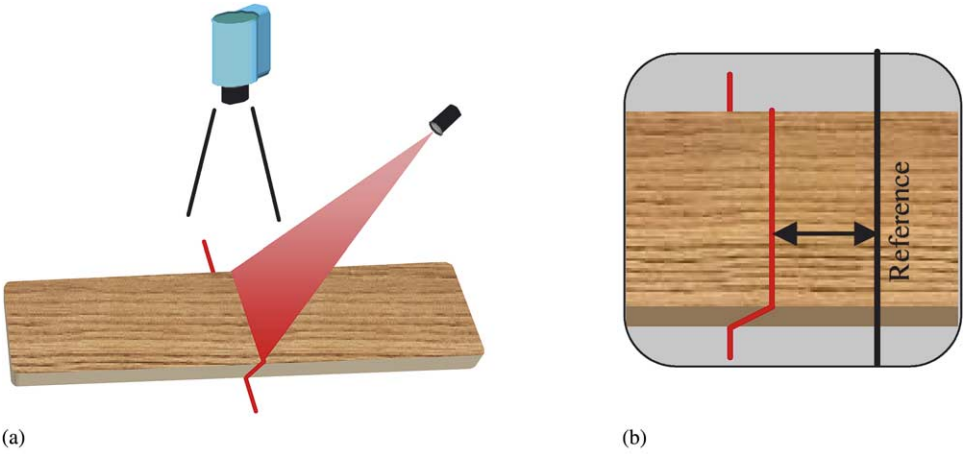

Fig. 2. Profile imaging geometry. (a) A camera is mounted vertically, looking downward at a board. A laser source generates a plane of light that is 45° relative to the horizontal. (b) From the camera's point of view, different board thicknesses cause the laser light to appear as a 2-dimensional curve in an image. Deviation of the light from a known reference line in the image is directly related to the thickness of the board.

In our prototype system, the profile laser is mounted at an angle of 45° relative to the direction of travel of the board. A digital camera is mounted vertically above the board, and can provide images for estimating board thickness. The digital camera that is used in this system is the MAPP 2200 'smart camera', developed by Forchheimer et al. (1992), and also described in Åstrand (1996). The unit captures images of 256 rows by 256 columns. Unlike conventional cameras, the internal MAPP (matrix array picture processor) sensor contains an on-board processor that is capable of manipulating complete rows of this array, in both digital and analog forms.

3. Noise effects

Profile images of rough hardwood boards suffer from various noise sources: noise from residual bark, debris, and dust; spatial quantization of the sensor array; sampling and quantization of intensity values; thermal sensor noise; and problems in thickness estimation due to variations in surface reflectance. Fig. 3 presents a typical example that illustrates several types of noise. Coordinates x and y represent the

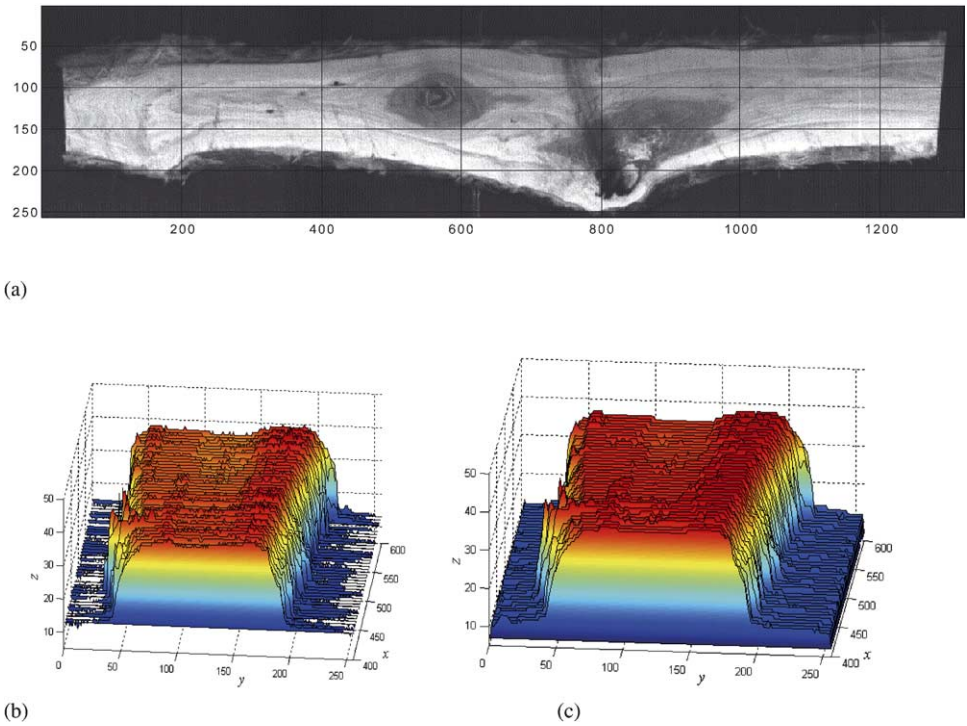

Fig. 3. Example of noise effects. (a) Intensity (reflectance) image of an unplaned board. (b) A portion of the profile image for this board. Only columns 400–600 are shown. (c) Smoothed version of profile image. All axes have units of 1.5875 mm (1/16 inch).

column and row axes, respectively. The entire intensity image (also called a reflectance or tracheid image, Lee et al., 1999) appears in Fig. 3a. A portion of the profile image for this board is shown in Fig. 3b, where the z axis represents thickness. For all three axes, one step represents 1.5875 mm (1/16-inch). Residual bark and debris contained in wane area make it difficult to detect wane boundaries with high accuracy. Unlike other noise sources, which can be addressed in many cases by applying smoothing filters, residual bark and debris are still prominent in the smoothed profile image (lower left corners of Fig. 3b and c). The effect of noise due to bark and debris is quite severe, and this presents the most challenging part of the wane detection problem from profile images. A close examination also reveals different average thickness values on the upper and lower parts of the board (Fig. 3a), resulting in an uneven profile. This appears to be related to variation in reflectance, possibly due to differences in surface orientation of the board relative to the camera.

4. Wane detection

4.1. Threshold-based methods

Simple threshold methods fail for most boards that we have tested due to the noise described above. For example, Fig. 4a illustrates a case in which a single threshold is computed for each column x of the profile image using

$$T(x) = \mu(x) - \sigma(x), \tag{1}$$

where $\mu(x)$ and $\sigma(x)$ are the mean value and standard deviation, respectively, for a given column x. Any pixel in the profile having a value less than $T(x)$ is declared to be a wane point. This method has several shortcomings, unfortunately, as indicated by the many incorrect wane regions shown as dark points in Fig. 4a. Debris or defects often elevate the threshold value above the clear-wood area of the board. Modifying Eq. (1), offsetting the threshold by more than one standard deviation, has also proven to be unsatisfactory.

Because of these problems, we considered a somewhat more sophisticated method for selecting a threshold. In this refined threshold method, a threshold value for the upper (or lower) half of column x is determined by

$$T(x) = \min(T_1(x),\ T_2(x) - \theta) \tag{2}$$

where T_1 is a threshold value selected at one standard deviation below the mean thickness value for this (half) column, and T_2 is another threshold value that corresponds to the mode (the highest peak) of the histogram $h(x)$ for that column, and θ is a constant selected empirically in the range $0 < \theta \leq 1$.

That is,

$$T_1(x) = \mu(x) - \sigma(x) \tag{3}$$

$$T_2(x) = \arg\max(h(x)). \tag{4}$$

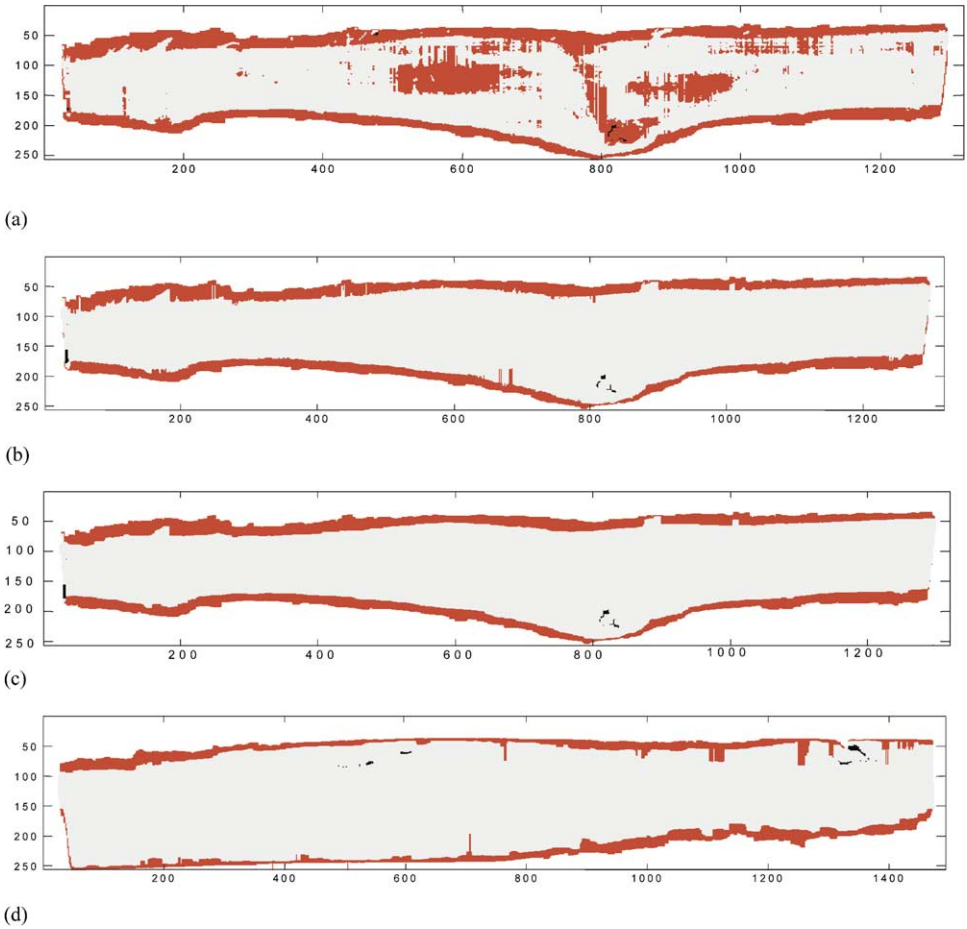

Fig. 4. Comparison of threshold methods for wane detection. (a) Simple threshold method (column-by-column processing), which fails in most cases. The threshold value is based on thickness statistics for each column. (b) Refined threshold method. (c) Further refinement. A median filter is applied to the wane edge positions on the previous image to obtain smoother wane contours. This final result is quite good. (d) Example for a different board, with poor results. Unfortunately, the selection of thresholds using statistical criteria has not resulted in a wane-detection method that is robust over many boards.

As described above, when debris appears in the wane area, T_1 is often higher than the value of the board surface, and this yields incorrect results. However, in such a case, T_2 typically gives more a reasonable answer. Operator arg max(·) finds the thickness value at which the histogram $h(x)$ has maximum value. Fig. 4b shows that this refined threshold method successfully avoids most undesired effects of the various noise sources. A median filter is then applied along the wane-edge positions of Fig. 4b to refine the wane contours (Fig. 4c). This has the effect of smoothing the wane contour and removing most of the outliers.

Although the second method works well for some boards, it fails to provide completely satisfactory results for others. A failure example is given in Fig. 4d, in which several 'spikes' remain in the wane boundaries.

4.2. Surface normal and curvature estimation

Because of problems encountered in finding a suitable threshold, we began to develop a method for wane detection that depends on surface properties such as orientation and curvature. Although it is possible to estimate these properties using discrete differences, we adopted a surface-fitting approach that is more robust in the presence of noise (see Hoffman and Jain, 1987, for additional discussion in the context of range data).

Similar to the approach described in Besl and Jain (1988), we model thickness as a function of two variables that is C^2-continuous, $z(x, y)$. As described previously, the variables x and y correspond to the column and row directions of profile images, respectively. A thickness value is estimated within a local 5×5 neighborhood (?) of the data points using classical least-squares fitting of a biquadratic polynomial:

$$z(x,\ y) = ax^2 + bx + cy^2 + dy + exy + f. \tag{5}$$

This results in local values for the coefficients, a, b, c, d, e, and f, to minimize the error criterion

$$E = \sum_{x_i,\ y_i \in \Omega} (z_i - \hat{z}_i)^2, \tag{6}$$

where $z_i = z(x_i,\ y_i)$ is the estimated analytical value and $\hat{z}_i$ is a corresponding measured thickness value.

Using this surface model, we proceed to determine surface orientation and curvature. The orientation of a surface is expressed in terms of the surface normal vector. The surface normal at a point $P = (x, y, z)^T$ is denoted by $\vec{n}_P$ (Carmo, 1976),

$$\vec{n}_P = (-z_x,\ -z_y,\ 1)^T \tag{7}$$

where the subscripts (x, y) of z represent partial derivatives. Therefore, we can explicitly write the surface normal with the estimated coefficients as follows:

$$\vec{n}_P = (-2ax - b - ey,\ -2cy - d - ex,\ 1)^T. \tag{8}$$

Surface curvature can be expressed in any direction within the tangent plane at a

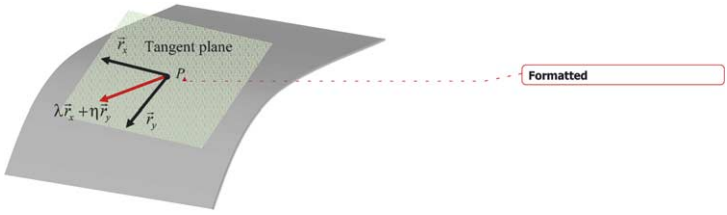

Fig. 5. Directions within a tangent plane at a surface point P.

surface point, $P = (x, y, z)^T$, as illustrated in Fig. 5. Let $\vec{r}_x$ and $\vec{r}_y$ represent any two different directions in the tangent plane. Then an arbitrary direction can be expressed as $\lambda\vec{r}_x + \eta\vec{r}_y$ and the surface curvature in this direction at the point P is given by (Faugeras, 1993)

$$\kappa(P) = \frac{\lambda^2 z_{xx} + 2\lambda\eta z_{xy} + \eta^2 z_{yy}}{n(\lambda^2(1 + z_x^2) + 2\lambda\eta z_x z_y + \eta^2(1 + z_y^2))}, \tag{9}$$

where $n = \sqrt{1 + z_x^2 + z_y^2}$. In our application, because wane is oriented in the x-direction, we consider only the y direction by designating $\vec{r}_x$ and $\vec{r}_y$ as the directions of the two image coordinate axes, and by setting $\lambda = 0$ and $\eta = 1$. The resulting curvature expression is

$$\kappa_y(P) = \frac{z_{yy}}{n(1 + z_y^2)} = \frac{z_{yy}}{\sqrt{1 + z_x^2 + z_y^2}(1 + z_y^2)} \tag{10}$$

Similarly, the y component of the surface normal is given by

$$n_y(P) = -z_y = -(2cy + d + ex) \tag{11}$$

4.3. Search criteria

For each column of a profile data, the algorithm searches for two wane boundaries corresponding to the two edges of the board. In each case, the search begins at a point within the wane region and proceeds toward the interior of the board. The following heuristics are used in the search:

1. Near the wane boundary, the y-component of the surface normal should be small in magnitude. This corresponds to a small rate of change along the column of the image, and can be represented as follows, where α is an empirically chosen constant:

$$|n_y(P)| < \alpha \tag{12}$$

2. Near the wane boundary, curvature in the y direction should be small in magnitude, with a value that is negative or zero. The requirement for small magnitude eliminates sharp peaks and valleys from consideration, which typically are caused by debris or residual bark. The requirement for a negative value corresponds to a surface that more closely resembles a peak than a valley, as we

expect for a wane boundary. This heuristic can be represented as follows, where β is also a constant:

$$\beta < \kappa_y(P) \leq 0 \tag{13}$$

Using only the first criterion, wane detection can fail when debris is present, as illustrated in Fig. 6. That is, the first criterion cannot distinguish some cases of debris from the flat surface of board. On the other hand, peaks caused by debris or residual bark typically exhibit high curvature. Therefore, the curvature-based criterion in Eq. (13) helps avoid such cases. Our approach is to search inward from the sides of the board until points satisfying both criteria are found. The resulting points typically provide good initial estimates of wane boundaries.

4.4. Adjustment

To perform the search described above, a least-squares fit of a biquadratic polynomial is computed for each data point in a column, and the criteria expressed in Eqs. (12) and (13) are evaluated using the resulting coefficients. Empirically, we found that this fitting procedure performs well when moderate noise is present, but not for many cases involving debris and residual bark. Because of this, we apply a 2-dimensional smoothing filter as a preprocessing step before doing the least-squares fit.

The preprocessing helps reduce the negative effects from debris and residual bark, but it also displaces edge positions by a small amount. To achieve better localization

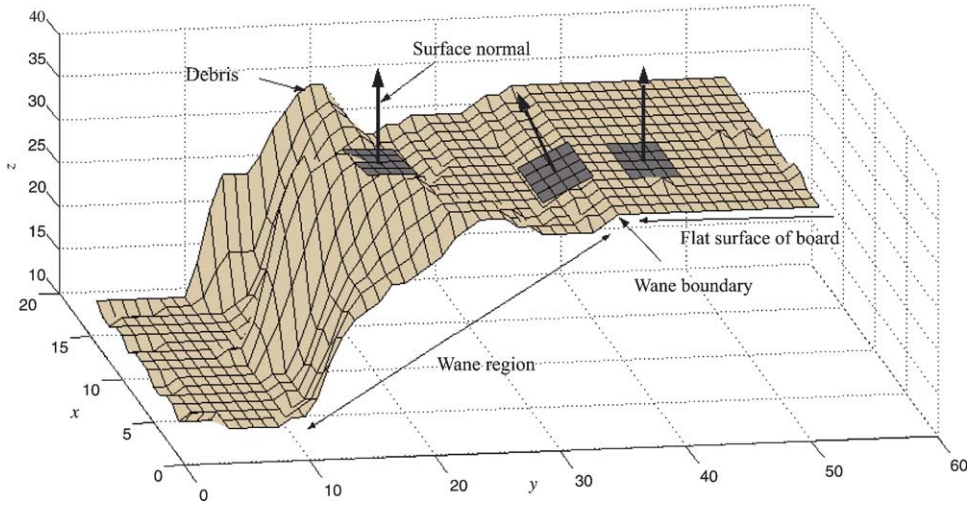

Fig. 6. Profile plot of several image columns. The wane region extends approximately from row 10 to row 40 in this example. Rows 0–10 represent background, and rows 40 and higher represent the sawn central portion of the board. Three surface normals are indicated by dark arrows. Detection of the wane boundary is made difficult because of the presence of bark and debris in the image.

of the wane boundaries, our algorithm searches the original image ($\hat{z}$) outward from the initial estimates. In this case, a discrete approximation of the second derivative is computed, and the first zero-crossing point is selected as the wane-boundary position. The second derivative in the column direction can be approximated as follows:

$$z_{yy}(x,\ y) \approx \hat{z}(x,\ y-1) - 2\hat{z}(x,\ y) + \hat{z}(x,\ y+1). \tag{14}$$

4.5. Further refinement

The method described above results in two wane-boundary positions per each column—one for each side of the board. However, each column is processed independently for improved processing speed. Because of this, it is often the case that adjacent columns are not in strict agreement. As a post-processing step, we reduce these undesirable effects by filtering the two wane-boundary curves. This can be done efficiently after finding the wane boundary for the entire board.

Denote one wane boundary as a one-dimensional signal $h(x)$, representing boundary location for each column x. Fig. 7a shows a small portion of the signal that contains an outlier. Then the median operation

$$\tilde{h}(x) = \text{median}(h(x)) \tag{15}$$

can be used to remove outliers. Here, the median is computed over a window of size $2d+1$, where we typically select $d = 2$. A filtered version of the signal is shown in Fig. 7b, where the outlier has been suppressed.

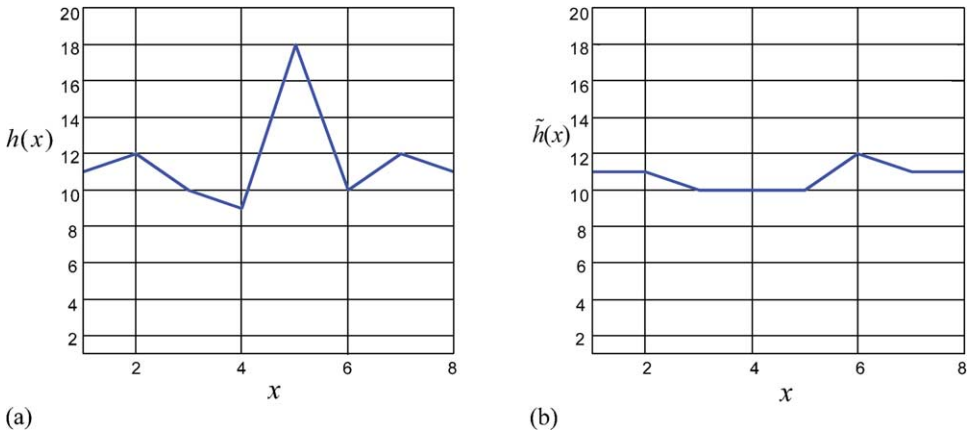

Fig. 7. Smoothing a wane boundary by median filtering. (a) Original data (8 points only) that contain an outlier at $x = 5$. (b) Filtered version of the previous data. The outlier has been suppressed.

5. Implementation and experimental results

We have tested the proposed method using profile data scanned with a prototype inspection system. To reduce noise, especially from debris and residual bark in the wane area, the system applies a 3×3 averaging filter as a preprocessing step. Fig. 8 shows a column of profile image. The dotted line represents original data and the solid line is its smoothed version. The scanning system produces integer height values for the profile image, but the outputs of the averaging filter are real valued. A median filter might be more appropriate than an averaging filter in this situation, but we chose the averaging filter for reasons of processing speed.

The wane-detection algorithm searches for the first point that satisfies both criteria (12) and (13) from a carefully selected 'start position' to the '1/3 position' (the point 1/3 of the board's width from the board edge). Arrows in Fig. 8 illustrates these points. The upper start position is selected in wane area by the procedure described below (and the procedure for lower start position is similar):

1) For the upper side of column x, select the 1/3 position, $y = l$. We assume that this point does not lie in the wane region, and can therefore serve as a reference height for the interior portion of the board.
2) Check that l is not a point in a split or hole by confirming $|\mu(x) - \hat{z}(x,\ l)| < \gamma$, for a suitable constant γ. If this is not the case, select another point that is nearer to the board edge and satisfies the above condition.

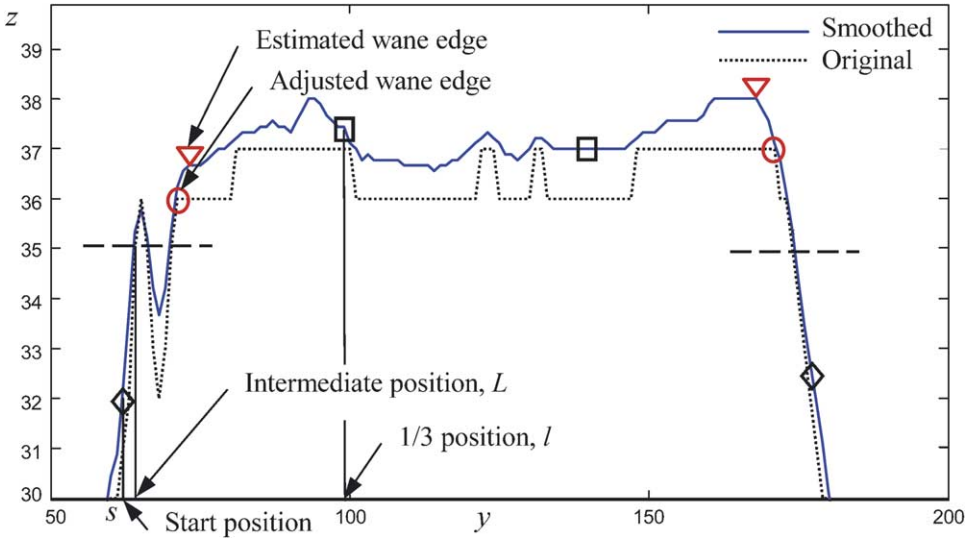

Fig. 8. Demonstration of the method using a profile plot for one column. The two ends of the column are processed separately. First, a point is carefully selected from the wane area (diamond mark). Second, a search is conducted toward the 1/3 position of the board (square mark) for a point that satisfies both search criteria. The triangle mark represents the wane edge that is found for this case. The adjustment step searches within a small neighborhood of the original data to find an improved wane edge (circle mark).

3) Find an intermediate position, L, which is the minimum row location from the set $\{y|s < y < l \quad \text{and} \quad |\hat{z}(x, y) - \hat{z}(x, l)| \leq 2\}$, where s is the outside edge of the board. This step avoids points in splits or holes to be possible start positions.
4) Select the start position (diamond mark in Fig. 8) as the maximum row location from the set $\{y|s < y < L \quad \text{and} \quad |\hat{z}(x, y) - \hat{z}(x, L)| \geq 2\}$.

Fig. 9 displays results of the proposed wane detection method. Applied to the same example board used in Fig. 4a, the method results in reasonable estimation of wane area for the board. It also shows that the adjustment step can eliminate some outliers as shown in Fig. 9a and b. Note that the estimated wane region in (a) is slightly thicker than the one in (b), as noted by the markings at column 400. This is due to the smoothing effect. Fig. 9c shows the final result after further refinement with median filtering along both wane boundaries. This compares favorably with the result for the same board given in Fig. 4c.

Fig. 10 shows another example, corresponding to the case given in Fig. 4d. Although the threshold-based methods performed very poorly for this board, the surface approximation method performs very well.

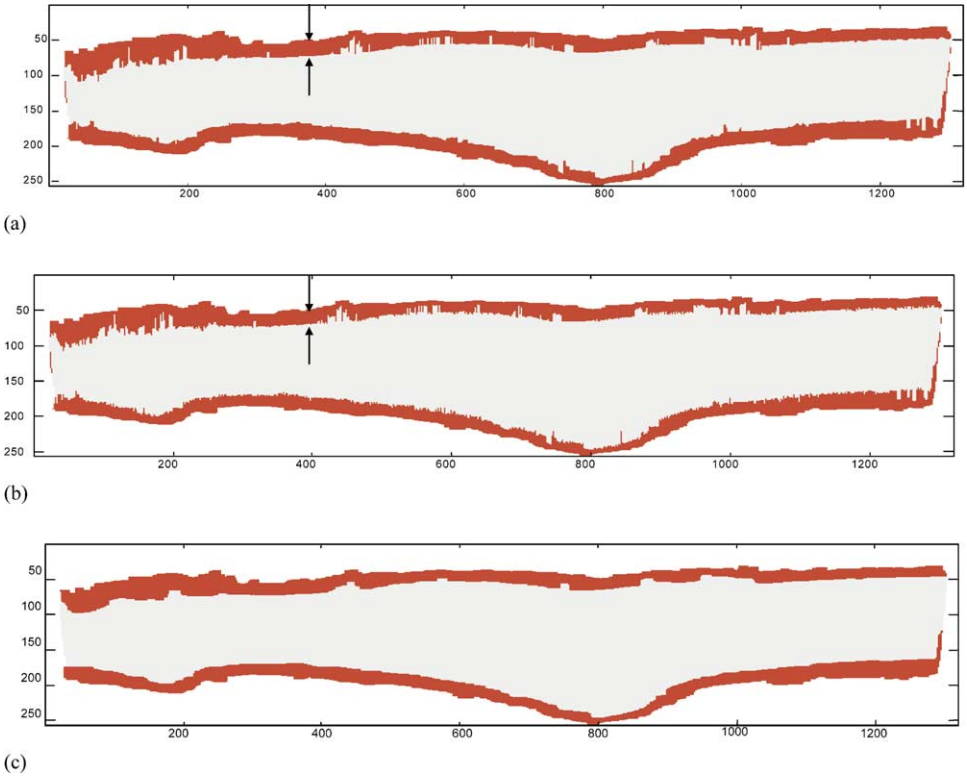

Fig. 9. Surface approximation method (a) without adjustment and (b) with adjustment. (c) Results of median filtering of (b) along both wane edges.

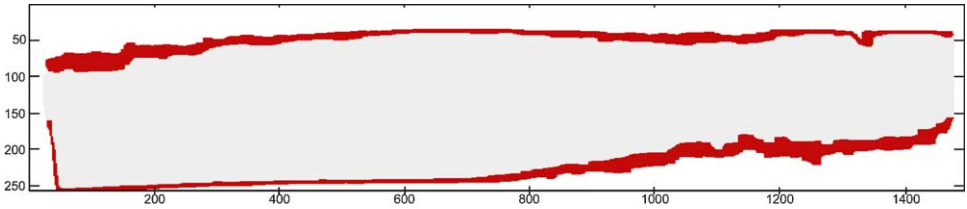

Fig. 10. Re-examination of the case in Fig. 4d. The surface approximation method gives superior results over the threshold methods that were considered.

6. Quantitative analysis

We manually determined wane boundary positions for two different rough lumber boards, and we used that information as ground truth in assessing the accuracy of two image analysis methods. Tables 1 and 2 show comparisons of the refined threshold method, formulated in Eq. (2), with the surface approximation method of the previous section. The average and standard deviation of absolute error between true and estimated wane boundaries have been calculated separately for the upper and lower sides of the two boards. The tables also indicate the percentage of outliers, which are defined as estimated wane boundaries that deviate more than 8 pixels (1/2 inch) from the actual locations.

For the first sample board, both methods produce good results as shown in Fig. 4c and Fig. 9c. Statistical results, summarized in the two tables, show that the surface approximation method is slightly better than the threshold method for this sample board. The surface approximation method is consistently better in terms of standard deviation of error and in the number of outliers. For average error, the refined threshold method is better for the upper wane boundary (3.1 vs. 2.3 pixels), but the surface approximation is better for the lower wane boundary (3.5 vs. 3.1 pixels).

For the second sample board, substantial differences are evident in the results for the two methods. The average error values for the surface approximation method (1.6 and 2.0 pixels for the upper and lower parts of the board, respectively) are less than half of those for the refined threshold method. The standard deviations of error are similarly better for the surface approximation method. The most dramatic result

Table 1
Quantitative evaluation for the refined threshold method

Refined threshold method	Sample board 1		Sample board 2	
	Upper	Lower	Upper	Lower
Average (pixel)	3.7	3.1	6.1	5.1
S.D. (pixel)	4.1	2.2	6.3	5.6
Outliers (%)	13.0	2.5	31.4	24.2

'Upper' and 'lower' refer to the two sides of the boards, as depicted in Fig. 3a. Average and standard deviation values are given in units of pixels, where each pixel represents 1.5875 mm (1/16 inch).

Table 2
Quantitative evaluation for the surface approximation method

Surface approximation method	Sample board 1		Sample board 2	
	Upper	Lower	Upper	Lower
Average (pixel)	2.3	3.5	1.6	2.0
S.D. (pixel)	3.0	2.0	1.4	2.9
Outliers (%)	8.1	2.1	0.07	6.3

of this comparison is the number of outliers; although the threshold method produces unacceptable numbers of outliers (31.4 and 24.2% for the upper and lower wane boundaries), the surface approximation method results in acceptable levels of 0.07 and 6.3%.

It is interesting to note that the surface approximation method yields better results for board 2 than for board 1 in nearly all respects, whereas the opposite is true for the refined threshold method. This is related to the larger amount of debris and residual bark that is present on the second board. The surface approximation method exhibits less susceptibility to this, and produces correspondingly better results.

Fig. 11 shows a comparison of the true wane boundaries and the estimated wane boundaries for board 1. Dotted curves in Fig. 11a represent the actual wane boundaries, obtained by visual inspection. Solid curves depict the wane boundaries estimated by the surface approximation method. As expected, higher absolute error is present near substantial amounts of debris or residual bark (Fig. 11b). This is particularly apparent for the upper part of the board near columns 100 and 1000, which are also illustrated by photographs in Fig. 12. In the upper portion of Fig. 12b, some of the residual bark has the same height as the sawn surface of the board.

Variations in laser intensity reflected by the board surface also account for some of the error. For example, a slightly higher reflectance was observed in the lower half of board 1, and this has resulted in somewhat higher estimated profile values than for the upper part of the board. This effect, which adversely affects the detection of the wane boundary, can be seen in the lower portion of Fig. 11b.

Fig. 13 shows a comparison of true and estimated wane boundaries for board 2. For this case, reflectance differences for the two halves of the board are not as obvious, and the major source of error is the presence of bark and debris within the wane region. As compared to board 1, this board has a steeper wane region, and its boundary is therefore easier to find.

7. Conclusion

We have implemented a technique to detect wane from profile images of rough lumber. The images are contaminated by a significant amount of noise, including

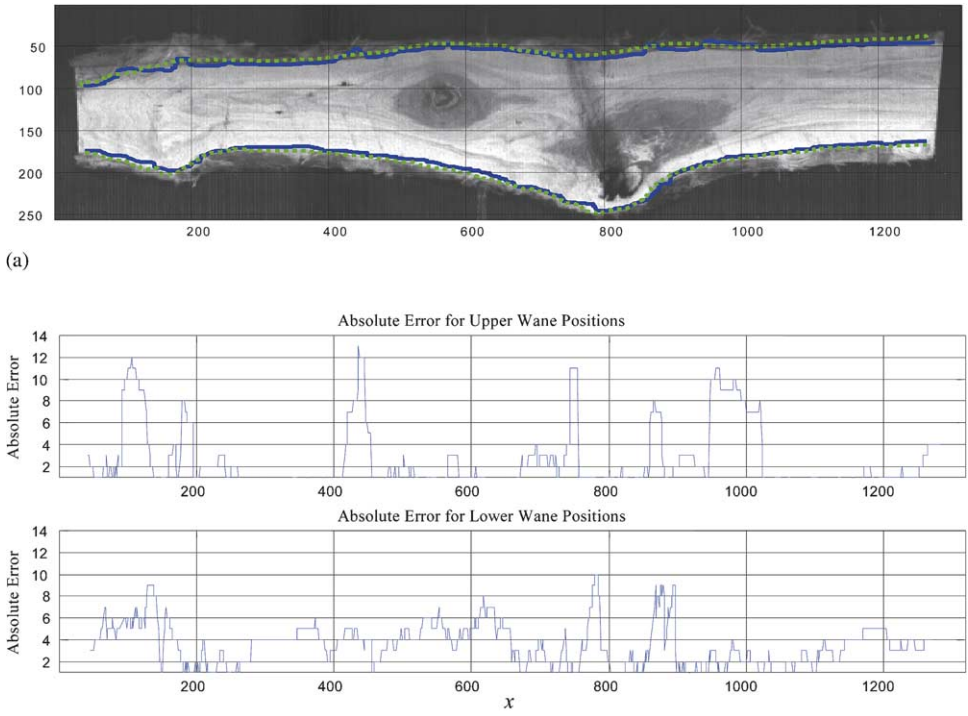

Fig. 11. Error analysis for sample board 1. (a) Dotted curve: true wane position. Solid curve: estimated wane position. (b) Absolute error for upper and lower sides of the board. For the upper part, residual bark and debris causes several large deviations in Table 2. For the lower part, variations in reflected laser intensity are a major source of error.

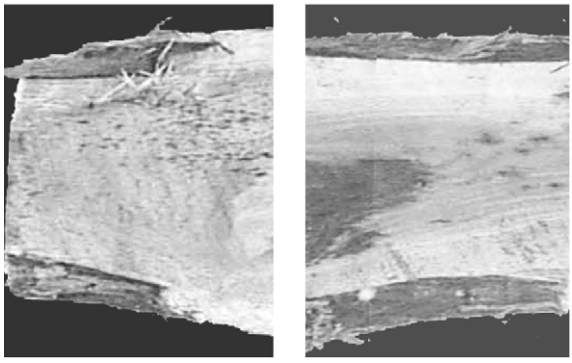

Fig. 12. Photos of the sample board 1 in black and white. Upper middle of these photos shows; debris around column 100 (a), and bark around column 1000 (b), respectively.

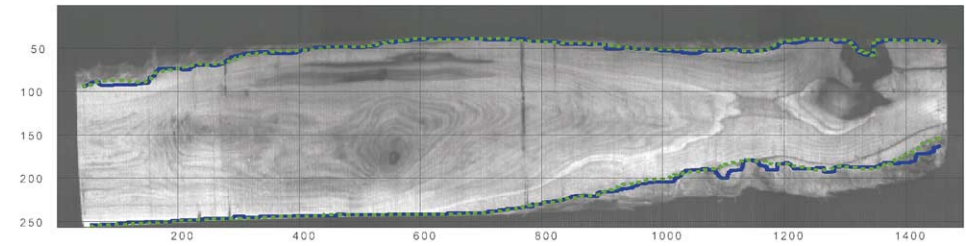

(a)

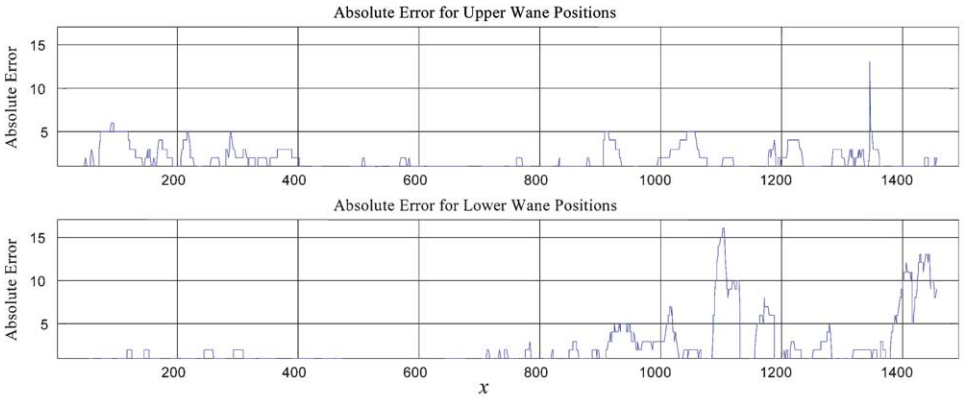

(b)

Fig. 13. Error analysis for sample board 2. The reflectance difference of each side of the board is not obvious, and therefore barks and debris are the major source of error.

noise from residual bark and debris. Because of the noise, simple threshold-based methods often yield poor results.

Our new algorithm is therefore based on an analysis of surface characteristics, particularly curvature and surface normal direction. It operates primarily on a column-by-column basis. Surface-based search criteria are used to identify crease edges that represent the boundaries of wane regions. We found that surface-normal direction alone is an inadequate source of information, often leading to incorrect wane boundaries because of bark and debris protrusions. With the incorporation of curvature information, however, the system is often able to avoid false detections due to bark and debris.

From some of the board profiles shown here (e.g. Fig. 6), it is clear that the detection of wane boundaries can be difficult even for human observers. In practice, of course, humans use additional cues such as color, grain direction, and recognition of surface characteristics to detect wane. For fast processing in automated systems, however, thickness measures resulting from laser profiling appear to be the best sources of data for detecting wane, and for identifying wood-deficit defects such as holes and cracks.

Acknowledgements

This work was partially supported by USDA Fund for Rural America Competitive Grant #97-36200-5274.

References

Åstrand, E., 1996. Automatic inspection of sawn wood. Ph.D. Dissertation, Department of Electrical Engineering, Linköping University, Linköping, Sweden.

Besl, J.P., Jain, R.C., 1988. Segmentation through variable-order surface fitting. IEEE Trans. Pattern Analysis and Machine Intelligence PAMI-10 (2), 167–192.

Carmo, M.P., 1976. Differential geometry of curves and surfaces. Prentice-Hall, Englewood Cliffs, NJ.

Cho, T.H., Conners, R.W., Araman, P.A., 1990a. A computer vision system for automated grading of rough hardwood lumber using a knowledge-based approach. Proceedings: IEEE International Conference on Systems, Man, and Cybernetics, November 4–7, Los Angeles, CA, pp. 345–350.

Cho, T.H., Connors, R.W., Araman, P.A., 1990b. A computer vision system for analyzing images of rough hardwood lumber. Proceedings: 10th International Conference on Pattern Recognition, vol. 1, June 16–21, Atlantic City, NJ, pp. 726–728.

Conners, R.W., Cho, T.H., Araman, P.A., 1989. Automated grading of rough hardwood lumber. In: Szymani, R. (Ed.), Proceedings: 3rd International Conference on Scanning Technology in Sawmilling, October 5–6, San Francisco, CA, pp. XVI-1–15.

Faugeras, O., 1993. Three-Dimensional Computer Vision: A Geometric Viewpoint. The MIT Press, Cambridge, MA.

Forchheimer, R., Ingelhag, P., Jansson, C., 1992. MAPP2200, a second generation smart optical sensor. In: Arps, R.B., Pratt, W.K. (Eds.), SPIE Proceedings, vol. 1659, pp. 2–11.

Hoffman, R., Jain, A.K., 1987. Segmentation and classification of range images. IEEE Transactions on Pattern Analysis and Machine Intelligence PAMI-9 (5), 608–620.

Lee, S.-M., Abbott, A.L., Schmoldt, D.L., 1999. Using an embedded-processor camera for surface scanning of unplaned hardwood lumber. In: Thompson, D.O., Chimenti, D.E. (Eds.), Review of Progress in Quantitative Nondestructive Evaluation, Plenum Press, New York, vol. 18, July 25–30, Montreal, Canada.